Research on deformed exotic nuclei by relativistic mean field theory in complex momentum representation

Xiao-Wei Wang and Jian-You Guo *

School of Physics and Materials Science, Anhui University, Hefei 230601, People's Republic of China

(Received 11 May 2021; accepted 5 October 2021; published 14 October 2021)

The exotic nuclei have attracted extensive attention in nuclear physics recently. The resonant states are thought to play a critical role at the formation of these exotic phenomena. Here, the complex momentum representation (CMR) method for resonances is combined with the relativistic mean field (RMF) theory applicable to deformed system. The RMF-CMR method for deformed exotic nuclei is established. The theoretical formalism and numerical details are presented. ^{75}Cr is chosen as an example, the energies and widths of single-particle levels and their evolutions to deformation β_2 are obtained for resonant states together with bound states. The available potential energy curve shows that ^{75}Cr is a deformed nucleus with $\beta_2 = 0.333$. Wave function of the orbit occupied by the last valence neutron consists mainly of d-wave components. The corresponding density represents a considerably diffuse distribution, which suggests that ^{75}Cr is a d-wave deformed halo nucleus. The predication is helpful to explore the deformation halos in experiment for the nuclei in the medium mass region.

DOI: 10.1103/PhysRevC.104.044315

I. INTRODUCTION

With the development of radioactive nuclear beam technologies, physicists have synthesized many nuclei far away from the valley of stability. In these nuclei, there appear many exotic phenomena, such as neutron (proton) halos (skins) [1,2], energy-level inversion [3,4], change of magic numbers [5–7], exotic radioactivity [8,9], and so on.

Among these exotic phenomena, halos embody the special characteristics of finite quantum many bodies, and attract the extensive attention of nuclear physicists. So far, many halo nuclei have been observed in experiments, such as neutron halo nuclei: ^{11}Li [10], ^{11,14}Be [11], ^{17,19}B [12], ^{19,22}C [13,14], and ^{23}O [15]; proton halo nuclei: ^{8}B [16], ^{9}C [17], ^{17}Ne [18], ^{20}Mg [19], ^{23}Al [20], ^{26,27,28}P [21], and deformed halo nuclei: ^{31}Ne [22,23], ^{37}Mg [24], and ^{29}F [25]. These halo nuclei are located at the vicinity of the neutron or proton drip line. The valence nucleons are close to the continuous threshold and are easy to be scattered into the continuum. The resonances in the continuum play important roles at the formation of these exotic phenomena [26,27]. Therefore, the exploration of resonances is the key to understanding the properties of exotic nuclei.

To explore resonances, physicists have developed many methods which include the R-matrix method [28,29], the S-matrix method [30,31], the Jost function approach [32,33], the Green's function method [34–37], the pseudostate method [38], the complex scaling method [39], and so on. These methods have achieved considerable success in handling unbound problems. For examples, the resonance and decay in the weakly bound and unbound three-body nuclei ^{9}Be, ^{26}O, and ^{16}Be are depicted excellently using the pseudostate method within the hyperspherical formalism [40,41]. The many-body resonances in light nuclei are described well with the complex scaling method in combination with the nuclear cluster model [42]. The experimental data on multiparticle scatterings, such as ^{6}He scattering on carbon and lead targets with the Coulomb breakup $^{6}\mathrm{He} \to {}^{5}\mathrm{He} + n \to {}^{4}\mathrm{He} + n + n$, are reproduced successfully with the complex scaled Green's function method [43]. Recently, the complex momentum representation (CMR) method has attracted additional attention for its success in dealing with unbound problems [44]. This method was first formalized by Berggren for the solutions of resonant states in Schrödinger equation [45]. Afterwards, the method was applied to different fields including the study of resonances in atomic and molecular systems [46] and atomic nuclei [47,48] in the nonrelativistic case. In combination with the shell model, the Gamow shell model was developed [49–51]. The Gamow shell model has achieved considerable success in describing exotic nuclei.

Due to the advantages of CMR, which describe the bound states and resonant states on an equal footing and is applicable to not only narrow resonances, but also broad resonances, we develop the CMR method to the relativistic framework for resonances in the spherical case [44] and obtain a better understanding of the pseudospin and spin symmetries in nuclear resonant states [52]. In combination with the relativistic mean field (RMF) theory, we have established the RMF-CMR in the relativistic meson exchange model [53] and the relativistic point-coupling model [54] and presented satisfactory descriptions for spherical exotic nuclei [55]. Considering that most of nuclei are deformed, to develop the theoretical formalism for deformed nuclei is interesting. In Ref. [56], we have developed the CMR method for deformed nuclei by solving Dirac equation in a phenomenological Woods-Saxon potential. To describe self-consistently the deformed exotic nuclei, it is necessary to develop the RMF-CMR applicable to deformed system.

*Corresponding author: jianyou@ahu.edu.cn

 ©2021 American Physical Society

At present, experimental and theoretical studies of halo nuclei are mainly focused on light nuclei, and some theories predict that halo or giant halo may exist in heavy nuclei. There are relatively few studies on the existence of halo in medium-mass nuclei. In Refs. [57,58], the exotic structure in medium-mass nuclei were investigated systemically by using the nuclear energy density functional theory, and the halo phenomena were predicted in the Cr and Sn isotopes near neutron drip line. In Ref. [59], the coupled-channel calculations are used to predict the halo heavier than ^{37}Mg, and several possible candidates of the neutron halo are suggested to be ^{71}Cr, ^{73}Cr, ^{75}Cr, ^{77}Fe, and ^{53}Ar. Similar to Ref. [59], the halos heavier than ^{37}Mg are explored by the complex momentum representation based on a simple Woods-Saxon potential, and ^{75}Cr, ^{77}Fe, and ^{53}Ar are suggested to be the possible candidates of neutron-halo nuclei [60].

In the paper, we first develop the RMF-CMR theory applicable to deformed nuclei. Then we apply the theory to investigate the exotic structure for the nuclei in the medium-mass region. ^{75}Cr is chosen as an example, we perform the RMF-CMR calculations self-consistently with quadruple deformation constraints to obtain the single-particle bound and resonant levels, configuration probabilities of the orbit occupied by the last valence nucleon and radial density distributions. Based on these results, we obtain the knowledge on the exotic structure in ^{75}Cr. The theoretical formalism is sketched in Sec. II. The numerical details and results are presented in Sec. III. A summary is given in Sec. IV.

II. FORMALISM

For the description of deformed exotic nuclei, we first introduce the theoretical formalism of the present model. The relativistic mean field theory describing the nuclei is based on an effective Lagrangian density constructed with the degrees of freedom that is associated with the nucleon field ψ, the meson fields σ, ω, ρ, and the photon field A. The effective Lagrangian density of the model [61–65] is written as

$$\begin{aligned}\mathcal{L} = \bar{\psi}\Big[&i\gamma^\mu\partial_\mu - M - g_\sigma\sigma - g_\omega\omega_\mu\gamma^\mu - g_\rho\vec{\rho}_\mu\vec{\tau}\gamma^\mu \\ &-\frac{1}{2}e\gamma^\mu(1-\tau_3)A_\mu\Big]\psi + \frac{1}{2}\left(\partial_\mu\sigma\partial^\mu\sigma - m_\sigma^2\sigma^2\right) \\ &-\frac{1}{4}\omega^{\mu\nu}\omega_{\mu\nu} + \frac{1}{2}m_\omega^2\omega^\mu\omega_\mu - \frac{1}{3}g_2\sigma^3 - \frac{1}{4}g_3\sigma^4 \\ &-\frac{1}{4}\vec{\rho}^{\mu\nu}\vec{\rho}_{\mu\nu} + \frac{1}{2}m_\rho^2\vec{\rho}^\mu\vec{\rho}_\mu + \frac{1}{4}c_3(\omega^\mu\omega_\mu)^2 \\ &+\frac{1}{4}d_3(\vec{\rho}_\mu\cdot\vec{\rho}^\mu)^2 - \frac{1}{4}A^{\mu\nu}A_{\mu\nu},\end{aligned} \tag{1}$$

here the tensors of the meson and photon fields are defined as

$$\begin{aligned}\omega^{\mu\nu} &= \partial^\mu\omega^\nu - \partial^\nu\omega^\mu, \\ \vec{\rho}^{\mu\nu} &= \partial^\mu\vec{\rho}^\nu - \partial^\nu\vec{\rho}^\mu, \\ A^{\mu\nu} &= \partial^\mu A^\nu - \partial^\nu A^\mu.\end{aligned}$$

M is the nucleon mass. g_σ, g_ω, and g_ρ are the coupling constants of σ, ω, and ρ mesons, respectively, with nucleons. g_2, g_3, c_3, and d_3 are the nonlinear self-coupling coefficients of mesons. Starting from the Lagrangian density, by using the classical variation principle, the Dirac equation describing the motion of nucleons is obtained as

$$[\vec{\alpha}\cdot\vec{p} + \beta(M+S) + V]\psi = \varepsilon\psi, \tag{2}$$

where $\vec{\alpha}$ and β are the Dirac matrices and S and V are the scalar and vector potentials. This set of Dirac equations can be solved self-consistently with the conventional methods, such as the basis expansion with the HO functions, or the finite element method in a finite box, the results describing the bound states can be obtained. The details can be seen in Refs. [61–65].

For these nuclei far from the valley of stability, the influence of resonant states is not negligible. To consider the contribution of resonant states, the physicists have developed many methods. Comparably, the complex momentum representation method holds many advantages indicated in Refs. [44,47]. For this reason, we transform the Dirac equation Eq. (2) into the momentum representation,

$$\int d\vec{k}'\langle\vec{k}|H|\vec{k}'\rangle\psi(\vec{k}') = \varepsilon\psi(\vec{k}), \tag{3}$$

where $H = \vec{\alpha}\cdot\vec{p} + \beta(M+S) + V$ is the Dirac Hamiltonian and $\vec{k} = \vec{p}/\hbar$ is the wave vector in the momentum representation.

For the axially deformed nuclei, the third component m_j of total angular momentum j and the parity π are good quantum numbers. The wave-function $\psi(\vec{k})$ can be expanded as

$$\psi(\vec{k}) = \psi_{m_j}(\vec{k}) = \sum_{lj}\begin{pmatrix} f^{lj}(k)\phi_{ljm_j}(\Omega_k) \\ g^{lj}(k)\phi_{\tilde{l}jm_j}(\Omega_k)\end{pmatrix}, \tag{4}$$

where $\tilde{l} = 2j-1$, $f^{lj}(k)$, and $g^{lj}(k)$ are the radial wave functions, $\phi_{ljm_j}(\Omega_k)$ is the angular wave function in the momentum representation,

$$\phi_{ljm_j}(\Omega_k) = \sum_{m_s}\left\langle lm\frac{1}{2}m_s|jm_j\right\rangle Y_{lm}(\Omega_k)\chi_{m_s},$$

with the spherical harmonics $Y_{lm}(\Omega_k)$ and the spin-wave function χ_{m_s}. m_s is the third component of spin angular momentum s.

Putting Eq. (4) into Eq. (3), the Dirac equation becomes

$$\begin{aligned}&Mf^{lj}(k) - kg^{lj}(k) + \sum_{l'j'}\int k'^2dk'V^+(l',j',p,q,l,j,m_j,k,k')f^{l'j'}(k') = \varepsilon f^{lj}(k), \\ &-kf^{lj}(k) - Mg^{lj}(k) + \sum_{l'j'}\int k'^2dk'V^-(\tilde{l}',j',p,q,\tilde{l},j,m_j,k,k')g^{l'j'}(k') = \varepsilon g^{lj}(k),\end{aligned} \tag{5}$$

where V^+ and V^- are as follows:

$$\begin{aligned}
&V^+(l', j', p, q, l, j, m_j, k, k') \\
&\quad = (-)^l i^{l+l'} \frac{2}{\pi} \int r^2 dr [V(r) + S(r)] j_l(kr) j_{l'}(k'r) \\
&\qquad \times \sum_{m_s} \langle lm|Y_{pq}(\Omega_r)|l'm'\rangle \left\langle lm\frac{1}{2}m_s|jm_j\right\rangle \left\langle l'm'\frac{1}{2}m_s|j'm_j\right\rangle, \\
&V^-(\tilde{l}', j', p, q, \tilde{l}, j, m_j, k, k') \\
&\quad = (-)^{\tilde{l}} i^{\tilde{l}+\tilde{l}'} \frac{2}{\pi} \int r^2 dr [V(r) - S(r)] j_{\tilde{l}}(kr) j_{\tilde{l}'}(k'r) \\
&\qquad \times \sum_{m_s} \langle \tilde{l}\tilde{m}|Y_{pq}(\Omega_r)|\tilde{l}'\tilde{m}'\rangle \left\langle \tilde{l}\tilde{m}\frac{1}{2}m_s|jm_j\right\rangle \left\langle \tilde{l}'\tilde{m}'\frac{1}{2}m_s|j'm_j\right\rangle.
\end{aligned} \tag{6}$$

For simplicity in computation, the Gauss-Legendre quadrature approximation is adopted. The integration in Eq. (5) is transformed into a sum $f(k_a)$ to k_a with the weight w_a, where k_a is the grid point of Gauss-Legendre quadrature. Furthermore, by the transformation $\mathbf{f}(k_a) = \sqrt{w_a}k_a f(k_a)$ and $\mathbf{g}(k_a) = \sqrt{w_a}k_a g(k_a)$, the Dirac equation becomes a symmetric matrix equation as

$$\begin{aligned}
&\sum_b \left[M\delta_{ab}\mathbf{f}^{lj}(k_b) + \sum_{l'j'} \sqrt{w_a w_b} k_a k_b V^+(l', j', p, q, l, j, m_j, k_a, k_b)\mathbf{f}^{l'j'}(k_b) - k_a\delta_{ab}\mathbf{g}^{lj}(k_b) \right] \\
&\qquad = \varepsilon \mathbf{f}^{lj}(k_a), \\
&\sum_b \left[-k_a\delta_{ab}\mathbf{f}^{lj}(k_b) - M\delta_{ab}\mathbf{g}^{lj}(k_b) + \sum_{l'j'} \sqrt{w_a w_b} k_a k_b V^-(\tilde{l}', j', p, q, \tilde{l}, j, m_j, k_a, k_b)\mathbf{g}^{l'j'}(k_b) \right] \\
&\qquad = \varepsilon \mathbf{g}^{lj}(k_a).
\end{aligned} \tag{7}$$

So far, the solution of Dirac equation Eq. (2) has become an eigenvalue problem of a symmetric matrix in Eq. (7). Different from Ref. [56], the present RMF-CMR is solved self-consistently with the scalar and vector potentials from the relativistic mean field. To obtain the potential-energy curve and the single-particle levels and their evolutions to deformation, the constrained RMF calculations are performed. The binding energy at a certain deformation is obtained by constraining the quadruple moment $\langle Q_2\rangle$ to a given value μ_2 in the expectation value of the Hamiltonian,

$$\langle H'\rangle = \langle H\rangle + \frac{1}{2}C_\mu(\langle Q_2\rangle - \mu_2)^2,$$

where C_μ is the constraint multiplier. The deformation parameter β_2 is obtained from the calculated quadruple moment $\langle Q_2\rangle$ [66].

III. NUMERICAL DETAILS AND RESULTS

With the preceding formalism, we explore the exotic structure for the nuclei near the drip line. In the relativistic mean field calculations, the parameter set NL3* [67] is adopted. The neutron-rich nucleus ^{75}Cr is taken as an example. We first perform the RMF calculations with the quadruple deformation constraints to obtain the potential-energy curve and the deformation of ground state. The Dirac equation is solved in real space with the truncated momentum $k = 4.0$ fm^{-1}. The other is the same as those in Fig. 2. Binding energy per nucleon E/A as a function of the quadruple deformation β_2 is displayed in Fig. 1. There appear two minima in the potential-energy curve. One locates at the prolate side with deformation $\beta_2 = 0.333$. Another one is on the oblate side with deformation $\beta_2 = -0.215$. Compared with the minimum on the oblate side, the minimum on the prolate side is lower, which means

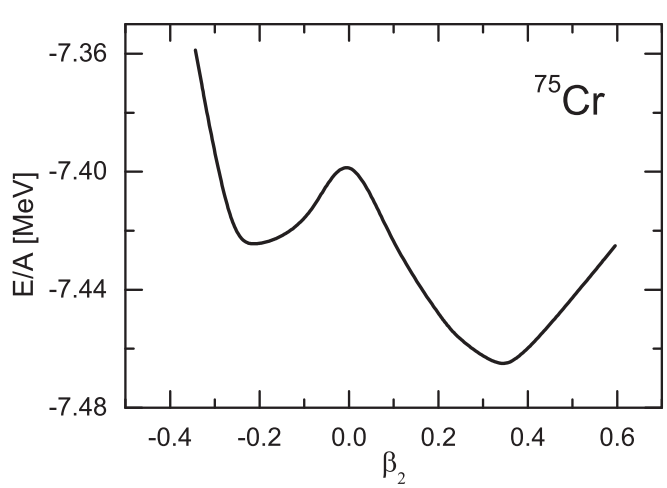

FIG. 1. The binding energy per nucleon E/A in ^{75}Cr and its evolution to the quadruple deformation β_2.

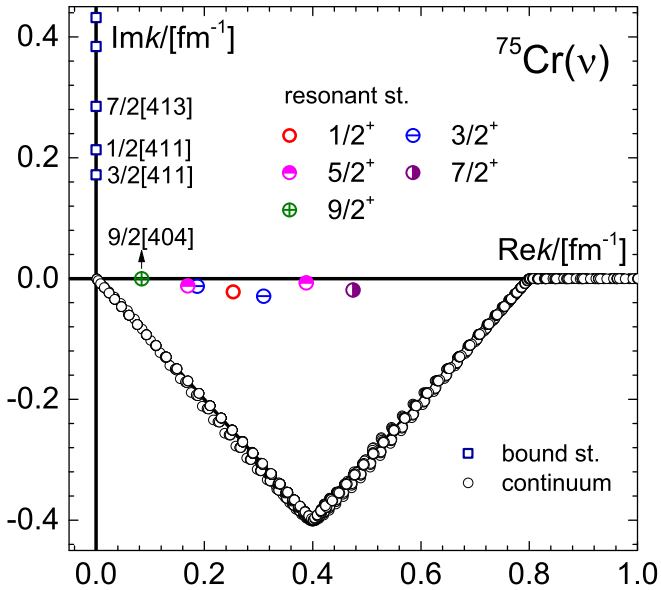

FIG. 2. The single-particle spectra in the deformed nucleus ^{75}Cr for states $\Omega^\pi = 1/2^+, 3/2^+, \ldots, 9/2^+$ on the complex momentum plane. The bound states and the continuous spectrum are marked with blue open boxes and black open circles, respectively. The resonant states with different quantum numbers are marked with different colored labels.

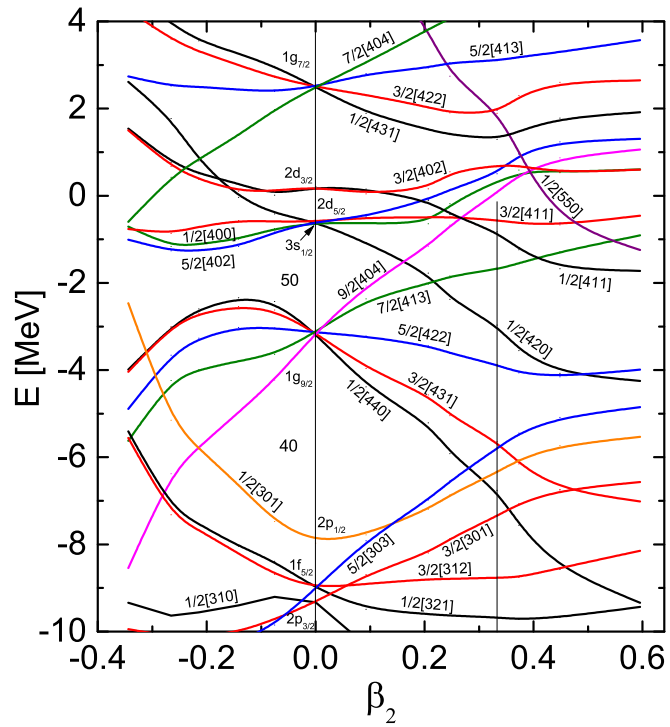

FIG. 3. The single-particle levels and their evolutions to the quadruple deformation β_2 in ^{75}Cr. These levels for axially deformed nuclei are labeled with the asymptotic quantum numbers $\Omega[Nn_z\Lambda]$. The corresponding spherical labels are placed in the position $\beta_2 = 0$. A shorter vertical line marks the location of the ground-state deformation with $\beta_2 = 0.333$. The numerical data are supplied as Supplemental Material [68].

the nuclei in the prolate minimum is the most stable. Hence, it can be convinced that ^{75}Cr is a prolate deformation nucleus with $\beta_2 = 0.333$ in its ground state.

With the knowledge on the deformation of the ground state, we explore the exotic structure in ^{75}Cr. First, we determine an appropriate integration contour in the RMF-CMR calculations to obtain all the resonant states concerned over the range of deformation considered. Similar to Ref. [56], the select contour is surrounded by the four points $k_1 = 0$, $k_2 = 0.4 - i0.4$, $k_3 = 0.8$, and $k_4 = 4.0$ fm^{-1}. The integration along the contour is performed by the Gauss-Legendre quadrature with 120 grid points. For every state with Ω^π, its wave function is expanded into eight spherical configurations. In the model space, the available single-particle spectra in the deformed nucleus ^{75}Cr with $\beta_2 = 0.333$ for states $\Omega^\pi = 1/2^+, 3/2^+, \ldots, 9/2^+$ are shown in Fig. 2.

From Fig. 2, it can be seen that all the bound and resonant states are clearly separated from the continuous spectrum. The bound states populate on the imaginary axis of momentum k, the resonant states are distributed in the fourth quadrant, and the continuous spectrum follows the integral contour on the complex momentum plane. For ^{75}Cr, there appear seven single-particle resonant states. Two of them are the resonant states with the quantum numbers $\Omega^\pi = 3/2^+$. Another two are the resonant states with $\Omega^\pi = 5/2^+$. The quantum numbers of the other three resonant states correspond to $\Omega^\pi = 1/2^+$, $7/2^+$, and $9/2^+$, respectively. All the resonant states are located near the real momentum axis, i.e., these resonant states are narrow resonances with long lifetimes.

In order to explore the exotic structure in the nucleus, we perform the RMF-CMR calculations with quadruple deformation constraints to obtain all the resonant states over the range of deformation considered. For ^{75}Cr, the available single-particle levels including the bound states and resonant states, and their evolutions to the deformation β_2 are plotted in Fig. 3. Because the valence nucleons are more likely to occupy the single-particle orbits near the Fermi surface, we only draw the resonant levels with the energy below 4.0 MeV, which is enough to discuss the physical issues concerned here. It can be seen from the figure that a clear shell structure appears in the bound levels as well as the resonant levels especially in the spherical case. Large gaps between the levels $1g_{9/2}$ and $2p_{1/2}$, and the levels $3s_{1/2}$ and $1g_{9/2}$ correspond to the traditional magic numbers 40 and 50. Moreover, there appears a large gap between the resonant levels $1g_{7/2}$ and $2d_{3/2}$, which looks forward to experimental verification. When the nucleus becomes deformed, the degenerate single-particle energy levels are undegenerate. Some levels fall with the increase indeformation, and the others rise. Several new gaps appear in these resonant levels, which is similar to that of the bound levels.

Based on the single-particle levels, we analyze the possibility of exotic structure in ^{75}Cr. It is known that there may appear exotic phenomena, such as halos if the valence nucleons occupy the weakly bound or resonant levels with lower angular momentum. From Fig. 3, it can be seen that the last (51st) valence neutron in ^{75}Cr occupies the level 5/2[402] in the range of $\beta_2 < 0.0$. This energy level is not only quite bound, but also has a large angular momentum, which results in a high eccentric barrier. Therefore, it is difficult to form a

halo for valence nucleon populating on the orbit. In the range of deformation $0.0 \leqslant \beta_2 \leqslant 0.175$, the last valence neutron occupies the level 1/2[420], which is developed from state $2d_{5/2}$ with the increasing deformation. The corresponding wave function consists mainly of the d-wave component and is not against the formation of a halo. Unfortunately, this is not the most stable state of ^{75}Cr, which can be figured out in the potential-energy curve in Fig. 1. In the range of deformation $0.175 \leqslant \beta_2 \leqslant 0.28$, the last valence neutron occupies the level 9/2[404] developed from the spherical wave $1g_{9/2}$, the wave function of this orbit is mostly composed of the $g_{9/2}$ component, which does not support the formation of a halo for the high centrifugal barrier. The same case appears in the range of deformation $0.395 \leqslant \beta_2 \leqslant 0.56$, the last valence neutron occupies the level 7/2[413] and does not favor the formation of a halo. In the range of deformation $0.28 \leqslant \beta_2 \leqslant 0.395$, the last valence neutron occupies the level 1/2[411]. From the potential-energy curve in Fig. 1, we know that ^{75}Cr is a prolate nucleus with deformation $\beta_2 = 0.333$. The last valence neutron occupies the weakly bound level 1/2[411] with the single-neutron separation energy S_n that is less than 1.0 MeV in the position, which satisfies the favorable condition of halo formation. Nevertheless, whether there is a halo phenomenon still needs further analysis.

To clarify the possibility of a halo, we examine the components of wave function for the single-particle orbit occupied by the last valence nucleon. The occupation probabilities of every configuration are defined as

$$P^i_{m_j} = P^{lj}_{m_j} = \int [f^{lj}(k)f^{lj}(k) + g^{lj}(k)g^{lj}(k)]k^2 dk, \qquad (8)$$

where $P^i_{m_j}$ represents the occupation probabilities of the configuration (lj). For the level 1/2[411], the eight configurations $s_{1/2}$, $d_{3/2}$, $d_{5/2}$, $g_{7/2}$, $g_{9/2}$, $i_{11/2}$, $i_{13/2}$, and $k_{15/2}$ are adopted in the RMF-CMR calculations. Occupation probabilities of these configurations are shown in Fig. 4. Since their imaginary parts are smaller than 10^{-12}, we only show the real parts of occupation probabilities there. In the range of deformation considered, the wave function of the single-particle state 1/2[411] consists mainly of these three configurations $d_{3/2}$, $d_{5/2}$, and $g_{7/2}$. The contributions of the other configurations are small. Comparably, the occupation probabilities of the configurations $d_{3/2}$ are dominant. At the position $\beta_2 = 0.333$, the occupation probabilities of the two configurations $d_{3/2}$ and $d_{5/2}$ are over 65%. Hence, the wave function of the ground state in ^{75}Cr is mostly composed of d components although the $g_{7/2}$ component has an important contribution.

Considering that the diffuse density distributions are a characteristic of a halo [26], we calculate the radial density distributions for these orbits occupied by valence nucleons with the following formula:

$$\rho_{m_j}(r) = \sum_{lj} [f^{lj}(r)f^{lj}(r) + g^{lj}(r)g^{lj}(r)], \qquad (9)$$

where $f^{lj}(r)$ and $g^{lj}(r)$ are the radial wave functions in coordinate representation obtained by transformation from momentum representation. The calculated radial density distributions for the single-particle level 1/2[411] are plotted in Fig. 5. For comparison, the radial density distributions of the three adjacent levels 3/2[411], 7/2[413], and 9/2[404] are also displayed there. For the bound level 7/2[413], the radial density distribution of the single-particle state is convergent. For the weakly bound level 3/2[411], the single-particle state has a diffuse density distribution. Similar to the level 3/2[411], the radial density distribution of the bound level

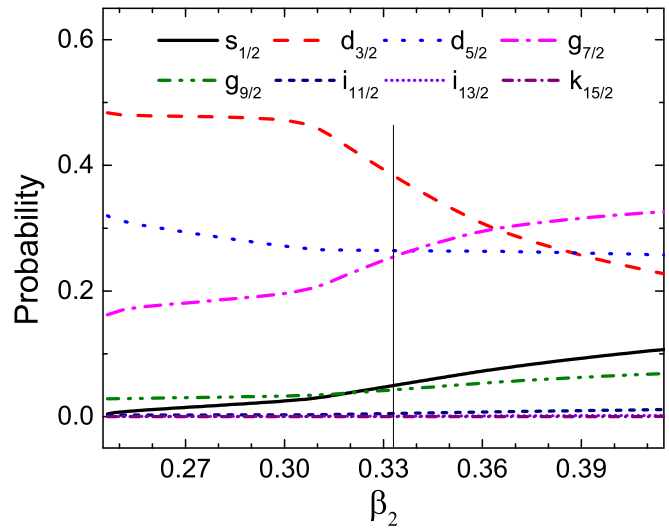

FIG. 4. Real part of the configuration occupation probabilities and their evolutions to the quadruple deformation parameter β_2. For the single-particle state 1/2[411], these configurations are $s_{1/2}$, $d_{3/2}$, $d_{5/2}$, $g_{7/2}$, $g_{9/2}$, $i_{11/2}$, $i_{13/2}$, and $k_{15/2}$ in the present calculations. The corresponding imaginary parts are too small on the order of 10^{-12} and not displayed here. The same as Fig. 3, a shorter vertical line marks the location of the ground-state deformation.

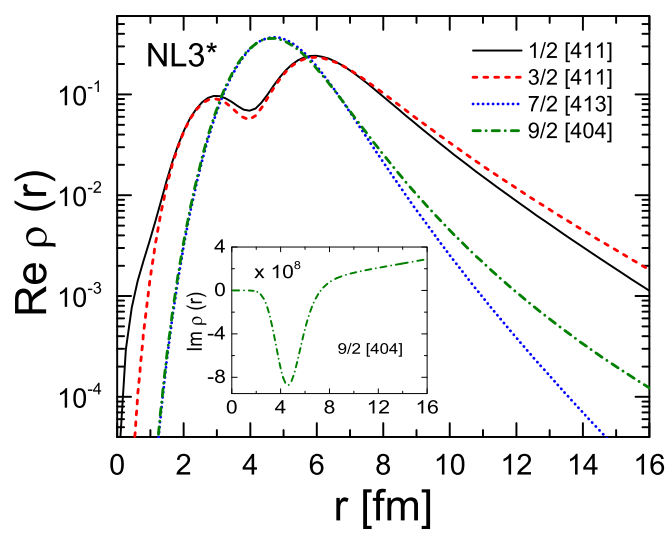

FIG. 5. Real part of radial density distributions for the single-particle states 1/2[411], 3/2[411], 7/2[413], and 9/2[404] in ^{75}Cr with deformation $\beta_2 = 0.333$. The insertion is the imaginary part of radial density distributions for the resonant state 9/2[404] multiplied by 10^8. The imaginary part of the three weakly bound states is at the power of 10^{-12} and not shown here.

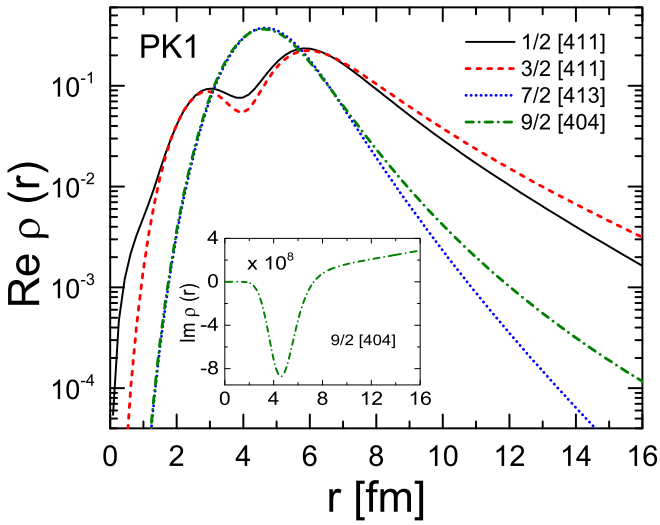

FIG. 6. The same as Fig. 5 but for the RMF-CMR calculations with the interactions PK1.

1/2[411], which is occupied by the last valence neutron, is considerably diffuse. As a consequence, we can conclude that a d-wave halo is likely to be formed in the deformed nucleus ^{75}Cr with the valence nucleon occupying the weakly bound level 1/2[411] at $\beta_2 = 0.333$. Compared with the bound levels 1/2[411] and 3/2[411], the radial density distributions of the level 9/2[404] are not very diffuse although it is a resonance state. These support that the valence nucleons occupying the weakly bound or resonant orbits with lower angular momentum is the condition of halo formation. In addition to these real parts, Fig. 5 also shows the imaginary part of radial density distribution multiplied by 10^8 for the resonant state 9/2[404] in insertion. The imaginary parts of the three bound states are not shown there because they are smaller than 10^{-12}. Compared with the real parts, the imaginary parts of radial density distributions are negligible for the four states shown in Fig. 5.

The same conclusion is obtained in the RMF-CMR calculations with the interactions PK1 [69], which can be seen in Fig. 6. Compared with the bound level 7/2[413], the radial density distributions of the weakly bound level 1/2[411] is more diffuse. The valence neutron populating on the orbit satisfies the favorable conditions for the formation of the halo. Moreover, the wave functions of the orbit is mostly composed of the d component. These indicate that the RMF-CMR calculations with the PK1 support a d-wave deformed halo nucleus for ^{75}Cr.

IV. SUMMARY

To summarize, the complex momentum representation method is combined with the relativistic mean field theory applicable to the axially symmetric system. The RMF-CMR model describing deformed nuclei is established. The model is applied to explore the exotic nuclei in the medium-mass region. ^{75}Cr is chosen as an example, the calculated potential energy curve shows that ^{75}Cr is a prolate deformed nucleus in its ground state.

In an appropriate integration contour of the complex momentum plane, the bound states, the resonant states concerned, and the continuous spectrum in the deformed nucleus ^{75}Cr are obtained in the self-consistent RMF-CMR calculations. All the bound and resonant states are clearly separated from the continuous spectrum. The bound states populate on the imaginary axis of momentum k, the resonant states are distributed in the fourth quadrant, and the continuous spectrum follows the integral contour on the complex momentum plane.

The RMF-CMR calculations with quadruple deformation constraints are performed, and the single-particle levels including the bound and resonant states and their evolutions to deformation are obtained. It is seen that there are clear shell structures in the single-particle bound levels as well as resonant levels in ^{75}Cr. Similar to the bound levels, there appear large gaps in the resonant levels in the spherical and deformed cases.

Combining knowledge of the potential-energy curve, the last valence neutron in ^{75}Cr should occupy the weakly bound orbit 1/2[411]. The calculated occupation probabilities show that the wave function of this orbit 1/2[411] consists mainly of the d-wave component. The radial density distribution of the single-particle orbit 1/2[411] is considerably diffuse. These show that ^{75}Cr is a d-wave-deformed halo nucleus with the valence nucleon occupying the weakly bound orbit 1/2[411]. The predication is helpful to explore exotic nuclei from experiment in the medium-mass region.

ACKNOWLEDGMENTS

This work was partly supported by the National Natural Science Foundation of China under Grants No. 11935001 and No. 11575002; the Key Research Foundation of Education Ministry of Anhui Province under Grant No. KJ2018A0028, and the Doctoral Scientific Research Startup Fund of Anhui University (Grant No. J01001319-J10113190082).

[1] I. Tanihata, H. Savajols, and R. Kanungo, Prog. Part. Nucl. Phys. **68**, 215 (2013).
[2] T. Nakamura, H. Sakurai, and H. Watanabe, Prog. Part. Nucl. Phys. **97**, 53 (2017).
[3] G. L. Wilson, W. N. Catford, N. A. Orr *et al.*, Phys. Lett. B **759**, 417 (2016).
[4] B. Longfellow, D. Weisshaar, A. Gade, B. A. Brown, D. Bazin, K. W. Brown, B. Elman, J. Pereira, D. Rhodes, and M. Spieker, Phys. Rev. Lett. **125**, 232501 (2020).
[5] A. Ozawa, T. Kobayashi, T. Suzuki, K. Yoshida, and I. Tanihata, Phys. Rev. Lett. **84**, 5493 (2000).
[6] R. F. Garcia Ruiz, M. L. Bissell, K. Blaum, A. Ekström, N. Frömmgen, G. Hagen, M. Hammen, K. Hebeler, J. D. Holt, G. R. Jansen, M. Kowalska, K. Kreim, W. Nazarewicz, R. Neugart, G. Neyens, W. Nörtershäuser, T. Papenbrock, J. Papuga, A. Schwenk, J. Simonis, K. A. Wendt *et al.*, Nat. Phys. **12**, 594 (2016).

[7] E. Leistenschneider, E. Dunling, G. Bollen, B. A. Brown, J. Dilling, A. Hamaker, J. D. Holt, A. Jacobs, A. A. Kwiatkowski, T. Miyagi, W. S. Porter, D. Puentes, M. Redshaw, M. P. Reiter, R. Ringle, R. Sandler, C. S. Sumithrarachchi, A. A. Valverde, and I. T. Yandow, Phys. Rev. Lett. **126**, 042501 (2021).
[8] E. Olsen, M. Pfützner, N. Birge, M. Brown, W. Nazarewicz, and A. Perhac, Phys. Rev. Lett. **110**, 222501 (2013); **111**, 139903(E) (2013).
[9] Y. G. Ma, D. Q. Fang, X. Y. Sun *et al.*, Phys. Lett. B **743**, 306 (2015).
[10] I. Tanihata, H. Hamagaki, O. Hashimoto *et al.*, Phys. Rev. Lett. **55**, 2676 (1985).
[11] M. Fukuda *et al.*, Phys. Lett. B **268**, 339 (1991).
[12] T. Suzuki *et al.*, Nucl. Phys. A **658**, 313 (1999).
[13] T. Nakamura, N. Fukuda, T. Kobayashi *et al.*, Phys. Rev. Lett. **83**, 1112 (1999).
[14] K. Tanaka, T. Yamaguchi, T. Suzuki *et al.*, Phys. Rev. Lett. **104**, 062701 (2010).
[15] C. Nociforo, K. L. Jones, L. H. Khiem *et al.*, Phys. Lett. B **605**, 79 (2005).
[16] M. H. Smedberg, T. Baumann, T. Aumann *et al.*, Phys. Lett. B **452**, 1 (1999).
[17] Z. H. Li *et al.*, Chin. Phys. Lett. **22**, 1870 (2005).
[18] A. Ozawa, T. Kobayashi, H. Sato *et al.*, Phys. Lett. B **334**, 18 (1994).
[19] T. Suzuki, H. Geissel, O. Bochkarev *et al.*, Nucl. Phys. A **616**, 286 (1997).
[20] A. Ozawa, K. Matsuta, T. Nagatomo *et al.*, Phys. Rev. C **74**, 021301 (2006).
[21] A. Navin *et al.*, Phys. Rev. Lett. **81**, 5089 (1998).
[22] K. Minomo, T. Sumi, M. Kimura, K. Ogata, Y. R. Shimizu, and M. Yahiro, Phys. Rev. C **84**, 034602 (2011).
[23] K. Minomo, T. Sumi, M. Kimura, K. Ogata, Y. R. Shimizu, and M. Yahiro, Phys. Rev. Lett. **108**, 052503 (2012).
[24] N. Kobayashi, T. Nakamura, Y. Kondo, J. A. Tostevin *et al.*, Phys. Rev. Lett. **112**, 242501 (2014).
[25] S. Bagchi, R. Kanungo, Y. K. Tanaka *et al.*, Phys. Rev. Lett. **124**, 222504 (2020).
[26] J. Meng and S. G. Zhou, J. Phys. G: Nucl. Part. Phys. **42**, 093101 (2015).
[27] S. G. Zhou, Phys. Scr. **91**, 063008 (2016).
[28] E. P. Wigner and L. Eisenbud, Phys. Rev. **72**, 29 (1947).
[29] G. M. Hale, R. E. Brown, and N. Jarmie, Phys. Rev. Lett. **59**, 763 (1987).
[30] J. R. Taylor, *Scattering Theory: The Quantum Theory on Nonrelativistic Collisions* (Wiley, New York, 1972).
[31] L. G. Cao and Z. Y. Ma, Phys. Rev. C **66**, 024311 (2002).
[32] B.-N. Lu, E.-G. Zhao, and S.-G. Zhou, Phys. Rev. Lett. **109**, 072501 (2012).
[33] B.-N. Lu, E.-G. Zhao, and S.-G. Zhou, Phys. Rev. C **88**, 024323 (2013).
[34] E. N. Economou, *Green's Function in Quantum Physics* (Springer-Verlag, Berlin, 2006).
[35] T. T. Sun, S. Q. Zhang, Y. Zhang, J. N. Hu, and J. Meng, Phys. Rev. C **90**, 054321 (2014).
[36] M. Shi, J. Y. Guo, Q. Liu, Z. M. Niu, and T. H. Heng, Phys. Rev. C **92**, 054313 (2015).
[37] X. X. Shi, M. Shi, Z. M. Niu, T. H. Heng, and J. Y. Guo, Phys. Rev. C **94**, 024302 (2016).
[38] O. I. Tolstikhin, V. N. Ostrovsky, and H. Nakamura, Phys. Rev. Lett. **79**, 2026 (1997).
[39] N. Moiseyev, Phys. Rep. **302**, 212 (1998).
[40] J. Casal and J. Gómez-Camacho, Phys. Rev. C **99**, 014604 (2019).
[41] J. Casal, M. Rodríguez-Gallardo, J. Arias, J. Gómez-Camacho, L. Fortunato, and A. Vitturi, SciPost Phys. Proc. **3**, 036 (2020).
[42] T. Myo, Y. Kikuchi, H. Masui, and K. Kato, Prog. Part. Nucl. Phys. **79**, 1 (2014).
[43] J. Carbonell, A. Deltuva, A. C. Fonseca, and R. Lazauskas, Prog. Part. Nucl. Phys. **74**, 55 (2014).
[44] N. Li, M. Shi, J. Y. Guo, Z. M. Niu, and H. Z. Liang, Phys. Rev. Lett. **117**, 062502 (2016).
[45] T. Berggren, Nucl. Phys. A **109**, 265 (1968).
[46] Y. K. Yang, Y. Wu, Y. Z. Qu, J. G. Wang, R. K. Janev, and S. B. Zhang, Phys. Lett. A **383**, 1929 (2019).
[47] G. Hagen and J. S. Vaagen, Phys. Rev. C **73**, 034321 (2006).
[48] A. Deltuva, Few-Body Syst. **56**, 897 (2015).
[49] R. J. Liotta, E. Maglione, N. Sandulescu, and T. Vertse, Phys. Lett. B **367**, 1 (1996).
[50] N. Michel, W. Nazarewicz, M. Ploszajczak, and K. Bennaceur, Phys. Rev. Lett. **89**, 042502 (2002).
[51] R. I. Betan, R. J. Liotta, N. Sandulescu, and T. Vertse, Phys. Rev. Lett. **89**, 042501 (2002).
[52] X.-X. Shi, Q. Liu, J.-Y. Guo, and Z.-Z. Ren, Phys. Lett. B **801**, 135174 (2020).
[53] K.-M. Ding, M. Shi, J.-Y. Guo, Z.-M. Niu, and H. Liang, Phys. Rev. C **98**, 014316 (2018).
[54] X.-N. Cao, K.-M. Ding, M. Shi, Q. Liu, and J.-Y. Guo, Phys. Rev. C **102**, 044313 (2020).
[55] X.-N. Cao, Q. Liu, Z.-M. Niu, and J.-Y. Guo, Phys. Rev. C **99**, 024314 (2019).
[56] Z. Fang, M. Shi, J.-Y. Guo, Z.-M. Niu, H. Liang, and S.-S. Zhang, Phys. Rev. C **95**, 024311 (2017).
[57] V. Rotival and T. Duguet, Phys. Rev. C **79**, 054308 (2009).
[58] V. Rotival, K. Bennaceur, and T. Duguet, Phys. Rev. C **79**, 054309 (2009).
[59] I. Hamamoto, Phys. Rev. C. **95**, 044325 (2017).
[60] X.-N. Cao, Q. Liu, and J.-Y. Guo, Phys. Rev. C **99**, 014309 (2019).
[61] B. Serot and J. D. Walecka, Adv. Nucl. Phys. **16**, 1 (1986).
[62] P. Ring, Prog. Part. Nucl. Phys. **37**, 193 (1996).
[63] D. Vretenar, A. V. Afanasjev, G. A. Lalazissis, and P. Ring, Phys. Rep. **409**, 101 (2005).
[64] J. Meng, H. Toki, S. G. Zhou, S. Q. Zhang, W. H. Long, and L. S. Geng, Prog. Part. Nucl. Phys. **57**, 470 (2006).
[65] T. Nikšić, D. Vretenar, and P. Ring, Prog. Part. Nucl. Phys. **66**, 519 (2011).
[66] P. Ring and P. Schuck, *The Nuclear Many-Body Problem* (Springer, Berlin, 1980).
[67] G. A. Lalazissis, S. Karatzikos, R. Fossion *et al.*, Phys. Lett. B **671**, 36 (2009).
[68] See Supplemental Material at https://link.aps.org/supplemental/10.1103/PhysRevC.104.044315 for the numerical data supplied.
[69] W. Long, J. Meng, N. Van Giai, and S.-G. Zhou, Phys. Rev. C **69**, 034319 (2004).